ARTICLE NO. 78-385R

Performance Evaluation of Gravity-Assisted Copper-Water Heat Pipes with Liquid Overfill

H. Nguyen Chi* and A. Abhat†
Institut für Kernenergetik und Energiesysteme, Universität Stuttgart, Stuttgart, Federal Republic of Germany

Extensive experimentation has been carried out with gravity-assisted copper-water screen wick heat pipes with liquid overfill. The presence of nucleate boiling and "impulse convection" during steady-state heat transfer in the pipes was established and boiling hysteresis was found to occur invariably. The maximum heat-transport capability was measured by varying several influence parameters, viz., operating temperature, inclination angle, fill charge, screen-wick mesh size, and number of screen layers. The limitation to the heat-transport capability is caused by the onset of film boiling in the evaporator zone. The correlation between $\dot{q}''_{max}$ and influence parameters is obtained using the theory of similarity. The correlation curve agrees with the experimental data within ± 10%.

I. Introduction

FOR a variety of terrestrial heat pipe applications, such as in energy conservation, heat recovery, solar energy utilization, etc., the heat pipe may be operated with gravity aid, i.e., with the condenser end elevated. Gravity forces thereby considerably augment the capillary forces for condensate return to the evaporator region and high heat transport capabilities can be realized. Moreover, due to the large pressure head available for liquid return, gravity-assisted heat pipes usually employ simple wick structures, e.g., screen wicks or axial/circumferential grooves, and for some applications, no wick structure at all. The latter type of heat pipe reduces to the well-known two-phase thermosyphon.

Presently, little is known of the exact thermal behavior and performance limitation of gravity-aided heat pipes. The limited research work available to date indicates that a large number of diverse factors may affect the heat pipe performance. In the low temperature range (20-90°C), Abhat and Nguyen Chi[1] have experimentally investigated the effect of tilt angle and fluid inventory on the performance of copper-water heat pipes lined with 1 and 2½ layers of 160-mesh screen wick. They established the role of nucleate boiling in influencing the steady-state performance and the maximum heat transport capability of the heat pipes. A comparison of their data with predictions obtained using liquid puddle models for nonwicked heat pipes (thermosyphons) proposed by Kaser[2] and Bienert[3] showed the latter to be inadequate for tilted wick heat pipes.

In the high temperature range (500-800°C), Kemme[4] has determined from tests with gravity-aided sodium and potassium heat pipes that a number of effects such as pressure gradient limitation, vapor pressure drop limitation, entrainment limitation, etc., may be responsible for performance limitation of the heat pipes. These limitations were further found to be influenced by the heat pipe geometry, wick structure, and working fluid properties.

Presented as Paper 78-385 at the 3rd International Heat Pipe Conference, Palo Alto, Calif., May 22-24, 1978; submitted July 6, 1978, revision received March 8, 1979.

Index categories: Heat Pipes; Conservation.

*Research Scientist.
†Leader, Solar Energy and Thermal Analysis Group.

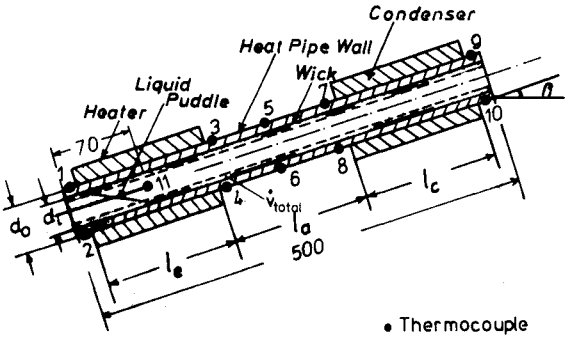

Fig. 1 Constructional details of the test heat pipes.

The present work is a continuation of that described in Ref. 1 and concerns itself with extensive experimentation with copper-water screen-wick heat pipes to determine the influence of several important parameters on the maximum performance of the heat pipes. The parameters considered and their range of variation are presented in Table 1. A thermosyphon of the same dimensions as the heat pipes is included in the test program to allow comparison between the maximum performance of wicked and nonwicked heat pipes. The data for limiting heat flux has been correlated using the theory of similarity.

II. Experimental Apparatus and Procedure

The heat pipes used in the experimental program are listed in Table 2, along with the specifications of the wick structure, fill charge used in the tests, liquid fill required to saturate the wick, and the amount of liquid overfill in the pipes. For the selected dimensions of the heat pipes, an overfill of 1 g approximately corresponds to a 1.0 cm vertical height of the liquid puddle within the pipe.

Figure 1 shows a schematic of the test heat pipes. All heat pipes were 500 mm long with evaporator and condenser lengths l_e and l_c, respectively, of 160 mm each. The heat pipes CW1*-CW6*‡ and the thermosyphon CW8* had a nominal diameter of 12.5 mm (11.5 mm i.d., 13.5 mm o.d.); the heat pipe CW7* had a slightly larger nominal diameter of 14.5 mm and was included in the program to investigate the influence of heat pipe diameter on performance.

‡The asterisk on the heat pipe code is used to distinguish the heat pipes used in the present program from those described in Ref. 1.

Table 1 Influence parameters and their range of variation

No.	Influence parameter	Range of variation
1	Temperature level of operation, T_{II}	20-70 °C[a]
2	Angle of inclination of the heat pipe with respect to the horizontal, β	5-86 deg
3	Liquid fill charge, m (corresponding liquid overfill in heat pipe)	4-15.6 g (1.1-10.1 g)
4	Screen wick mesh size, N	50, 160, 250
5	Number of screen mesh layers, n	1, 2, 4, 6

[a] The temperature level of operation was restricted to this range and intentionally kept below the optimum level for water heat pipes due to the limitation of the heater capacity.

Ten NiCr-Ni thermocouples were attached to the heat pipe wall at the locations shown in Fig. 1 to monitor the wall temperature in the axial and radial directions. One additional thermocouple was inserted in the vapor space of the evaporator section of the pipes CW3*, CW5*, CW7* and CW8* at a distance of 70 mm from the evaporator end to allow computation of the wall superheat. The temperatures were measured using a 12-point chart recorder. During the later stages of experimentation, the wall temperature T_2 and vapor temperature T_{II} of pipes CW7* and CW8* were continuously monitored using a 2-channel strip chart recorder.

III. Visual Observations of the Heat-Transfer Phenomenon within Gravity-Aided Heat Pipes

Earlier work with the copper-water heat pipes showed evidence of strong nucleate boiling within the evaporator zone of the heat pipes.[1] To allow visual observations of the boiling phenomenon, a "half-heat pipe" comprised of a half-copper cylinder closed with a plexiglas cover was constructed. Figure 2 shows a schematic of the heat pipe along with the location of the thermocouples. The heat pipe was lined with two layers of 160-mesh wick on the inside of the copper surface. It was filled with 7 g of bidistilled water (overfill = 3 g) and tested at a tilt angle of 5 deg to the horizontal. Under no-load condition, the liquid overfill formed a distributed pool along the bottom surface of the evaporator zone.

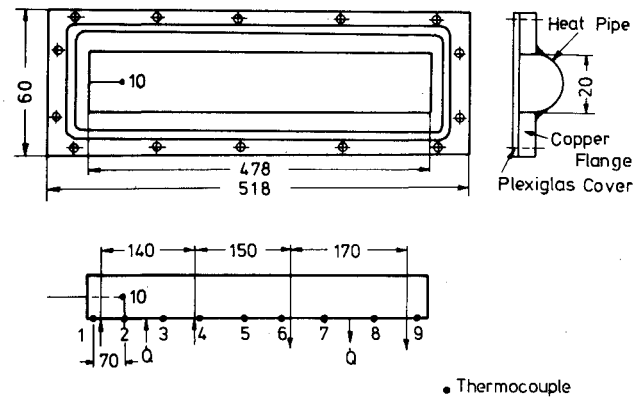

Fig. 2 Constructional details of the plexiglas-cover heat pipe and location of thermocouples.

Visual observations made with the plexiglas-cover heat pipe and data obtained for the wall superheat as a function of heat flux input confirmed the presence of nucleate boiling in the liquid pool collected in the evaporator section. The heat-transfer behavior of this pipe was similar to that for the other heat pipes and is discussed in the next section, along with the results for the heat pipe CW7*.

IV. Steady-State Performance of the Test Heat Pipes

Figure 3 shows the temporal variation of the evaporator wall temperature T_2 and vapor (saturation) temperture T_{II} for the heat pipe CW7* for step increments in the heat flux input $\dot{q}''$, as obtained with a 2-channel strip chart recorder. Figure 4, on the other hand, presents the axial wall temperature profile for the selected step increments in $\dot{q}''$, while Fig. 5 shows the variation of the wall superheat ΔT_s with $\dot{q}''$ for steady-state heat pipe operation. The wall superheat in Fig. 5 is calculated as $\Delta T_s = T_2 - T_{II}$, where T_2 is the wall temperature in the evaporator section and T_{II} is the vapor temperature. The data presented in these diagrams are taken with the heat pipe filled with 6.8 g of water (overfill = 2.6 g) operating at a tilt angle of 10 deg. Under no-load conditions, the liquid overfill forms a distributed pool along the bottom surface of the evaportor zone, as in the case of the plexiglas-

Table 2 Heat pipe specifications and liquid inventories used during experimentation

Heat pipe code	Screen wick mesh size	No. of screen layers	Wick thickness, mm	Fill charge, g	Saturated wick liquid charge, g	Overfill, g
CW1*	160	1	0.12	4.0	1.2	2.8
				6.6	1.2	5.4
				8.1	1.2	6.9
				10.3	1.2	9.1
CW2*	160	2	0.25	6.6	3.1	3.5
CW3*	160	4	0.44	6.3	5.2	1.1
				7.9	5.2	2.7
				11.0	5.2	5.8
CW4*	160	6	0.75	10.3	9	1.3
				13.3	9	4.3
				16.1	9	7.1
CW5*	50	2	0.75	11.0	8.4	2.6
				11.8	8.4	3.4
				12.9	8.4	4.5
				15.6	8.4	7.2
CW6*	250	2	0.15	6.5	1.8	4.7
				9.2	1.8	7.4
				11.9	1.8	10.1
CW7*[a]	160	2	0.25	6.8	4.2	2.6
CW8*[b]		nonwicked		8.7		

[a] The heat pipe CW7* has a nominal diameter of 14.5 mm (13.5 mm i.d., 15.5 mm o.d.).
[b] CW8* is a thermosyphon with a nominal diameter of 12.5 mm (11.5 mm i.d., 13.5 mm o.d.).

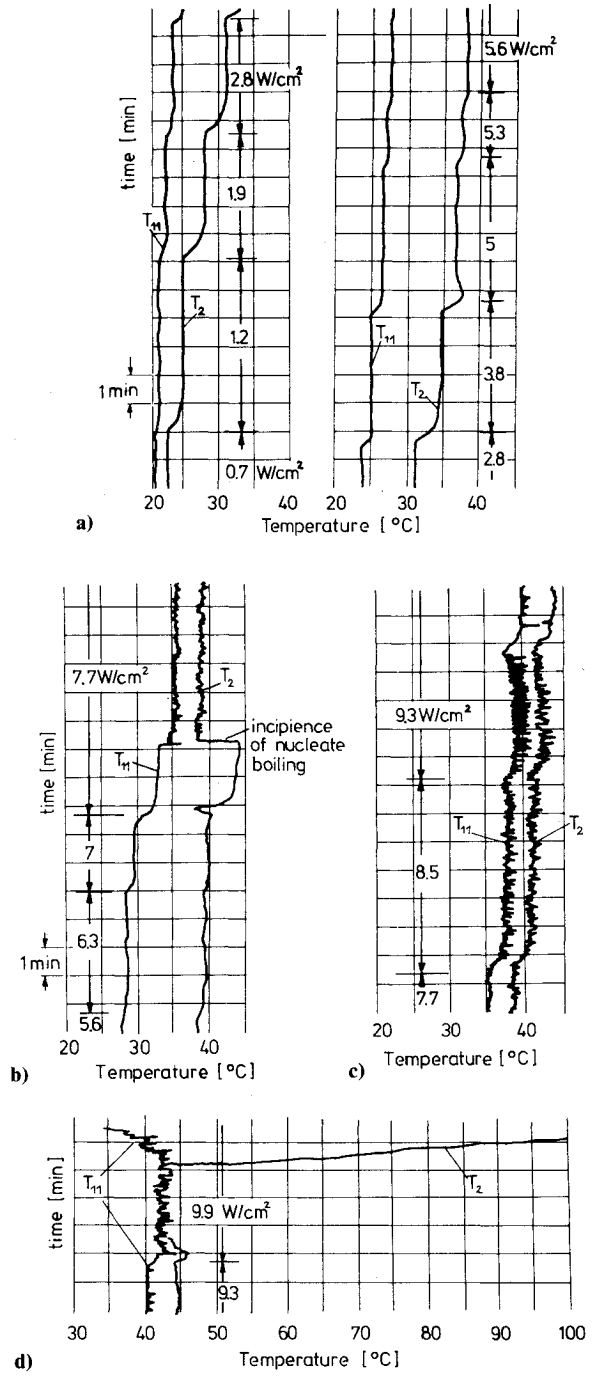

Fig. 3 Variation of wall and vapor temperature T_2, T_{11} as a function of time for various heat fluxes, heat pipe CW7*, $m = 6.8$ g, $\beta = 10$ deg. a) Natural convection regime; b) transition to nucleate boiling regime; c) nucleate boiling regime; d) departure from nucleate boiling.

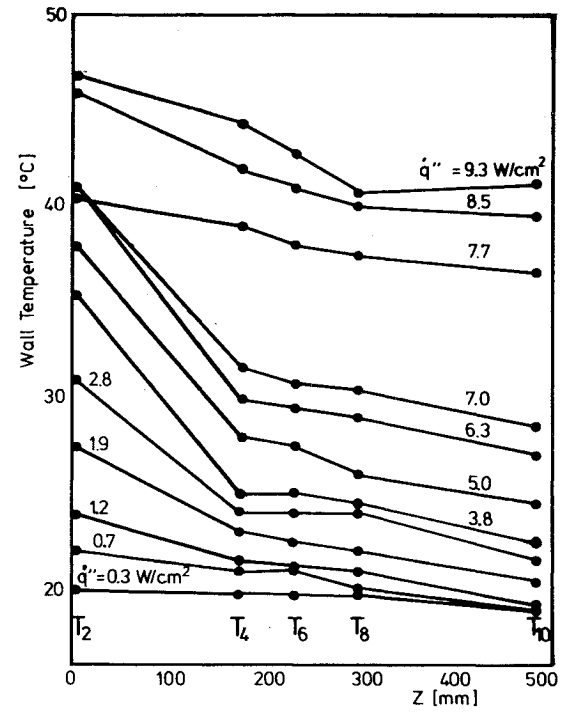

Fig. 4 Axial wall temperature profile for various heat fluxes, heat pipe CW7*, $m = 6.8$ g, $\beta = 10$ deg.

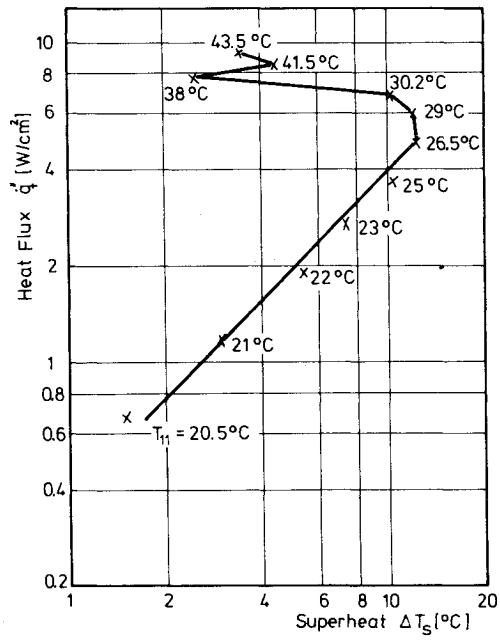

Fig. 5 Boiling curve, heat pipe CW7*, $m = 6.8$ g, $\beta = 10$ deg.

cover heat pipe. During the tests, the coolant temperature at the inlet of the heat pipe condenser was maintained constant at 20 °C. The vapor temperature, therefore, varied with increase in heat flux input $\dot{q}''$. For $\dot{q}'' < 7.0$ W/cm^2, the vapor temperature increased slowly from 20 to 30 °C; for $\dot{q}'' > 7.0$ W/cm^2, however, the vapor temperature shot up rather rapidly. The values of T_{11} measured at each of the data points are indicated in Fig. 5.

Based on the measurements, the heat transfer mechanism within the heat pipe may be characterized by four different regions, which are indicated in Figs. 3 and 5 and are described later. Similar regions were also identified during the measurements and visual observations made with the plexiglas-cover heat pipe.

A. Region I—Natural Convection Regime: $\dot{q}'' \leq 5.6$ W/cm^2

At these levels, the heat transfer is by natural convection in the liquid pool accompanied by heat conduction across the saturated wick in the remaining evaporator area. The data in this region are correlated by a line of slope 1 in the log-log plot of Fig. 5. Furthermore, Fig. 4 shows that the axial temperature gradient along the heat pipe wall increases with $\dot{q}''$.

B. Region II—Transition to Nucleate Boiling: $5.6 < \dot{q}'' < 7.7$ W/cm^2

This region is characterized by the transition to nucleate boiling. The axial temperature gradient along the heat pipe somewhat reduces during heat transfer in this region as seen in

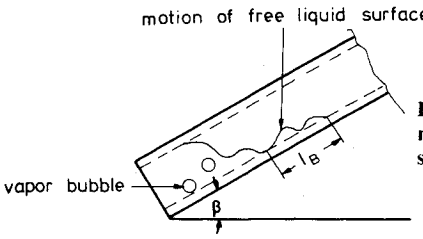

Fig. 6 Model for the motion of the free liquid surface.

Fig. 4 and no fluctuations in the wall and vapor temperatures are present. The incipience of boiling occurs at $\dot{q}'' = 7.7$ W/cm^2 and is marked by a sharp reduction in the wall superheat.

C. Region III—Nucleate Boiling: $7.7 \leq \dot{q}'' \leq 9.3$ W/cm^2

Nucleate boiling is well established in this range of heat flux. The nucleate boiling phenomenon was also visually observed with the plexiglas-cover heat pipe, and vapor bubbles were seen rising only in the distributed liquid pool. At a particular instant, a rough bubble count showed about 60 bubbles/min rising in the pool. Furthermore, waves were seen at the free surface of the liquid pool and periodic upward and downward motion of the interface was observed. The waves are created by the rising bubbles which break at the liquid-vapor interface imparting their kinetic and surface energies to the free liquid surface. The waves transport this energy by their propagation in the direction of the heat pipe wall, where they are reflected back at an angle equal to the angle of incidence. The energy dissipated at the free surface causes it to move up the heat pipe wall by a distance l_B (Fig. 6), such that the gain in potential energy due to the new elevated position of the free liquid surface equals the dissipated energy. The motion of the interface is governed by the frequency of the rising bubbles, so that a periodic upward and downward motion of the free liquid surface results.

Figure 3 shows fluctuations in the vapor temperature T_{11} and wall temperature T_2 following commencement of boiling. These fluctuations are typical of nucleate boiling heat transfer. They could additionally be caused by the periodic upward and downward motion of the liquid-vapor interface, the effect of which is enhanced due to the employment of the pipe of small diameter. Figure 3 further shows that as the heat flux is raised above 7.7 W/cm^2, the amplitude of the fluctuations increases while the frequency decreases. The higher amplitude possibly results from a larger bubble departure diameter at higher heat fluxes,[5] which affects the periodicity of the motion of the liquid-vapor interface. Furthermore, drawing an analogy with pool boiling, the product of bubble departure diameter and frequency is constant,[6] so that the frequency reduces.

D. Region IV—Departure from Nucleate Boiling: $\dot{q}'' > 9.3$ W/cm^2

At a heat flux of 9.9 W/cm^2, a very small wall superheat was measured, implying enhanced heat transfer within the evaporator region due to intense boiling. After a few minutes of steady-state operation, however, the wall temperature T_2 shot up at an extremely rapid rate of 60°C/min, whereas the vapor temperature and the wall temperatures in the adiabatic and condenser regions experienced a reduction. The sudden increase in the wall temperatures T_1 and T_2 is caused by the onset of film boiling in the liquid pool region, which terminates the steady-state operation of the heat pipe. A simultaneous reduction in the vapor temperature T_{11} and wall temperatures $T_3 \ldots T_{10}$ is measured.

Experiments with all heat pipes indicated a thermal behavior as discussed previously through the example of CW7*, and it could be concluded that heat pipe limitation was a consequence of the onset of film boiling in the liquid pool region. In addition, the well-known boiling hysteresis

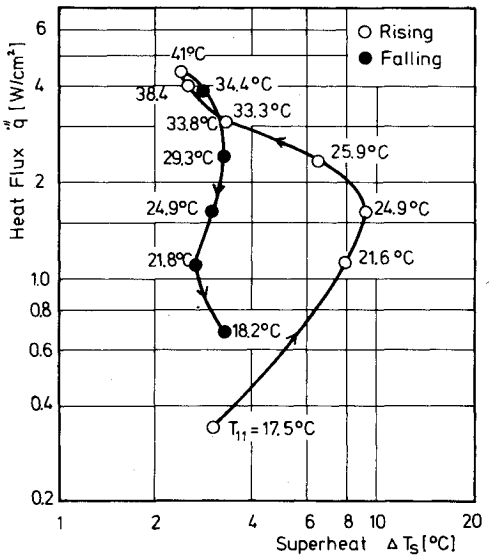

Fig. 7 Hysteresis boiling curve for increasing and decreasing heat flux, heat pipe CW3*, $m = 7.9$ g, $\beta = 10$ deg.

phenomenon was invariably exhibited by all heat pipes during their steady-state operation. A typical boiling curve that includes hysteresis effects is presented in Fig. 7 for the heat pipe CW3* (tilt angle = 10 deg, fill charge = 7.9 g). The shape of the rising and falling curves on this diagram is due to the variation of the vapor temperature with heat addition and reduction. The vapor temperature is, however, the same for a given heat flux input on the rising and falling curves.

V. Maximum Heat Transport Capability

A. Governing Phenomenon

The influence of nucleate and film boiling on the limitation of steady-state performance of the gravity-aided heat pipes has been described in the preceding section. For heat pipes with overfill, another effect influences their thermal behavior. The returning condensate only partially vaporizes along the saturated wick region of the evaporator, while the rest arrives at the liquid puddle with a finite velocity. Assuming that the liquid molecules behave elastically, the kinetic energy of the condensate molecules is set free and an elastic impulse is imparted to the molecules in the liquid pool, putting them into motion. We term this effect as "impulse convection." The impulse convection augments the heat transfer due to pool boiling in the evaporator region and accelerates the shearing off of the bubbles from the heated wall, so that a higher maximum heat transport capability is realized. The maximum heat flux capability $\dot{q}''_{\max}$ may then be written as

$$\dot{q}''_{\max} = f(\dot{q}''_{B,cr}, \dot{q}''_{IC}) \tag{1}$$

where $\dot{q}''_{B,cr}$ is the critical radial heat flux in the heat pipe due to the onset of film boiling in the liquid pool and $\dot{q}''_{IC}$ is the heat flux due to impulse convection. In general, nucleate boiling is a much stronger effect. However, for gravity-assisted heat pipes, where large heat-transport capabilities can be realized and flow velocity of the returning condensate can be large, impulse convection may play a significant role.

Comparisons between data obtained during the present investigations and computations made using the pool boiling correlation of Kutateladze[7] show the values of $\dot{q}''_{\max}$ for the gravity-assisted heat pipes to be considerably smaller than the critical heat flux density that occurs during pool boiling. This variation is largely attributed to the employment of pipes of small diameter in our experiments, whereby the liquid volume in the puddle is very small in comparison to the liquid volume used in normal pool boiling experiments. On the other hand,

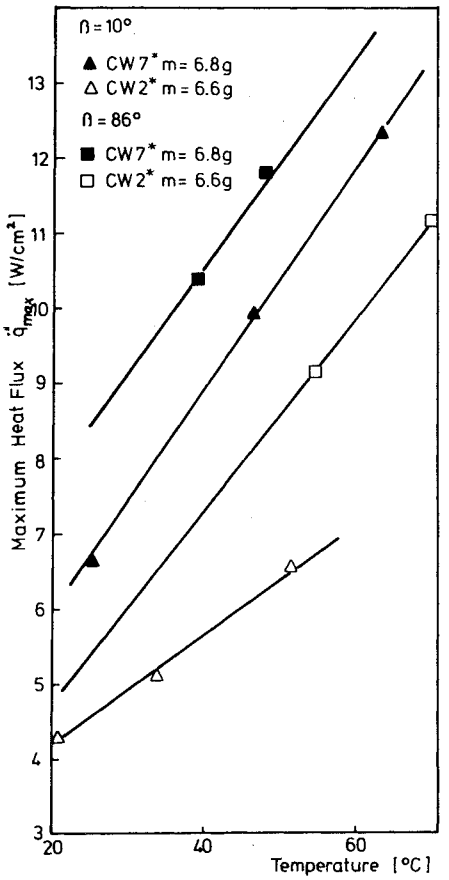

Fig. 8 Comparison of critical heat flux values of heat pipes with various diameters.

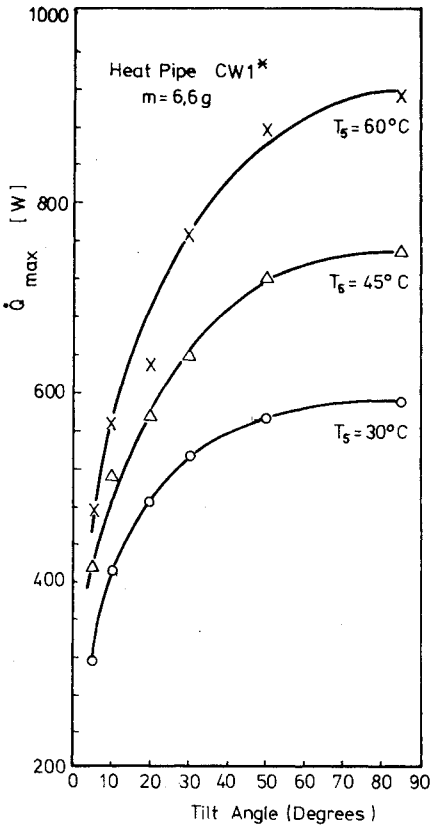

Fig. 9 Influence of tilt angle on maximum heat-transfer capability for various operating temperatures.

the area of the heat input surfaces in a heat pipe is relatively large. Thereby, a higher bubble density, and hence vapor volume, per unit liquid volume in the puddle exists in a heat pipe at any given heat input rate. This effect would accelerate the onset of film boiling so that a smaller critical heat flux density results.

How important an influence is exerted by the pipe diameter was established by including heat pipe CW7* of nominal diameter 14.5 mm in the test program (nominal diameter of other heat pipes = 12.5 mm, see Table 2). The pipe was tested with a liquid overfill of 2.6 g. Figure 8 provides a comparison of $\dot{q}''_{max}$ for the heat pipes CW7* and CW2* for tilt angles of 10 and 86 deg. For a heat pipe operating temperature of 40 °C, an increase in $\dot{q}''_{max}$ by about 50% is measured for a pipe diameter increase of only 2 mm. Further quantitative verification of the hypothesis through tests with heat pipes of different diameters is presently being carried out.

B. Role of Influence Parameters and Data Correlation

The various influence parameters considered in the investigations and their range of variation has been provided earlier in Table 1. We shall now examine the individual effect of each of these parameters and provide a data correlation based on the theory of similarity.

Tilt Angle, β

Figure 9 presents the dependence of the maximum heat transport capability $\dot{Q}_{max}$ of heat pipe CW1* as a function of tilt angle β for three different operating temperatures of 30, 45, and 60°C. The fill charge is 6.6 g. The maximum heat flow rate $\dot{Q}_{max}$ increases with the tilt angle β, the effect being particularly marked for $\beta < 50$ deg.

The gravity-assisted heat pipes operate with the aid of capillary and gravity forces, which influence the total volume flow rate of condensate, $\dot{V}_{total}$ returning to the evaporator zone (see Fig. 1). For heat pipes operating with liquid overfill, the returning condensate has a finite velocity at the free surface of the liquid surface in the liquid pool in the heat pipe, the magnitude of which influences the extent of impulse convection in the pool. The total volume flow rate corresponding to the limiting heat flux is written as

$$\dot{V}_{total} = [\Delta P_{cap} + \Delta P_{gravity}]\,(KA/\mu_l l_{eff})$$

$$\text{with } \Delta P_{cap} < \Delta P_{cap,max} \tag{2}$$

where ΔP_{cap} and $\Delta P_{gravity}$ are the available capillary and gravity heads, K is the wick permeability, A is the cross-sectional area for liquid flow, μ_l is the liquid viscosity and l_{eff} is the effective length of the heat pipe. For these conditions, an explicit relationship between $\dot{q}_{max}$ and $\dot{V}_{total}$ is not available. Instead, we have

$$\dot{q}''_{max} = f(\dot{V}_{total}) \tag{3}$$

The magnitudes of $\dot{V}_{total}$ are computed using Eq. (2) and plotted against the limiting heat flux $\dot{q}''_{max}$ in Fig. 10. A linear relationship is observed on the log-log plot so that the following correlation is obtained:

$$\dot{q}''_{max} = C_l\,(\dot{V}_{total})^{0.424} \tag{4}$$

Fill Charge, m

The influence of fill charge m, on the maximum heat flow rate $\dot{Q}_{max}$ for the heat pipe CW1* tested at a tilt angle of 86 deg is presented in Fig. 11. The plot shows that the amount of overfill exerts only a weak influence on $\dot{Q}_{max}$ in the range considered. Physically, the effect of overfill can be identified by two factors:

1) The total volume of liquid in the puddle, V_p, which can be spread over the whole length of the heat pipe depending on

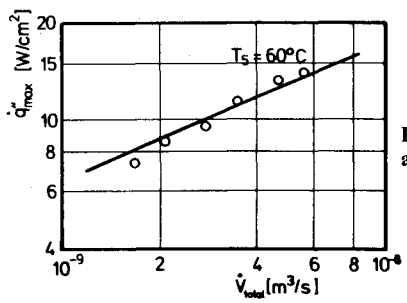

Fig. 10 Critical heat flux as a function of $\dot{V}_{total}$.

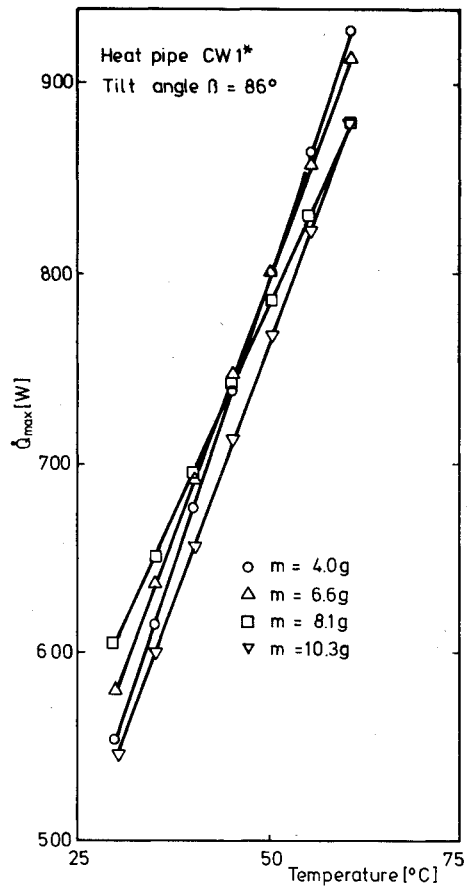

Fig. 11 Influence of fill charge on maximum heat-transport capability.

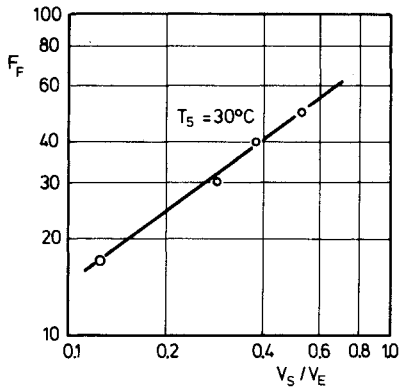

Fig. 12 Correlation between F_F and ratio (V_S/V_E).

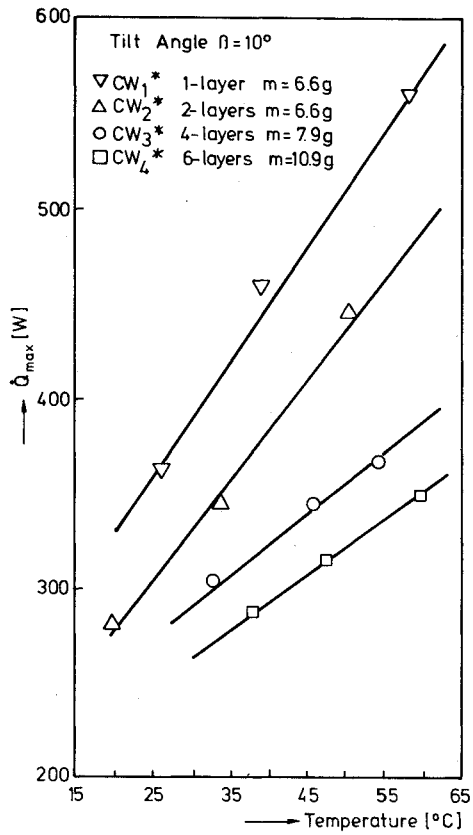

Fig. 13 Influence of number of screen layers on maximum heat-transport capability.

the tilt angle of operation. The magnitude of V_P influences the impulse convection effect in the pool: the smaller the pool volume V_P, the larger the expected impulse convection effect and an improvement in the heat-transfer rate follows. Thus we have, $\dot{q}''_{max} \alpha (1/V_P)$.

2) The liquid volume in the evaporator region, V_S. Bubbles are present in the liquid puddle contained in the evaporator region during heat pipe operation and influence the maximum heat-transfer rate, $\dot{q}''_{max}$. The total bubble volume in the liquid puddle is the governing criterion and depends on the magnitude of V_S or on the nondimensional ratio V_S/V_E, where V_E is the total evaporator volume. For the conditions in the heat pipe, a weak proportional dependence between $\dot{q}''_{max}$ and (V_S/V_E) could be assumed.

Combining the influences of β and m on $\dot{q}_{max}$, we obtain

$$\dot{q}''_{max} = C_2 (\dot{V}_{total})^{0.424} (1/V_P) (V_S/V_E)^{n_2} \quad (5)$$

or

$$F_F = \frac{\dot{q}''_{max} V_P}{(\dot{V}_{total})^{0.424}} = C_2 \left(\frac{V_S}{V_E}\right)^{n_2} \quad (6)$$

The variation of F_F with (V_S/V_E) is seen to be linear from the log-log plot of Fig. 12. From Fig. 12, we calculate the exponent n_2 to be 0.727.

Number of Screen Mesh Layers, n

Figure 13 shows the data for $\dot{Q}_{max}$ as a function of operating temperature for four different heat pipes (CW1*, CW2*, CW3* and CW4*) having the same wick mesh size ($N = 160$ mesh) but different number of screen mesh layers ($n = 1$, 2, 4 and 6, respectively). The heat pipe tilt angle is 10 deg. Figure 13 indicates that the maximum heat transport capability $\dot{Q}_{max}$ decreases with the increase in number of screen mesh layers n.

We have stated earlier that the presence of bubbles in the liquid puddle region affects the maximum heat-transfer rate. Bubbles are generated at the heat pipe wall and grow in the voids in the screen mesh. A vapor bubble departs from the wick structure when the buoyancy force overcomes the friction and adhesion forces in the screen wick. The friction force is the governing factor and is proportional to the wick

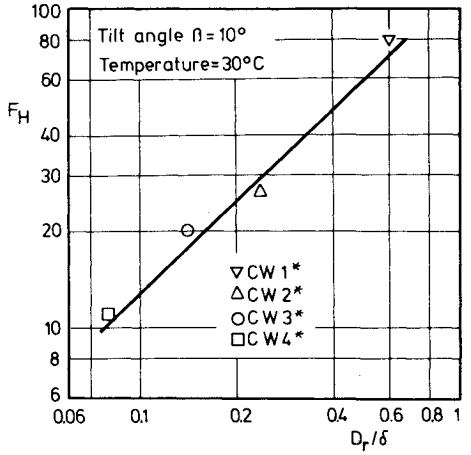

Fig. 14 Correlation between F_H and ratio of wire diameter and wick thickness (D_r/δ).

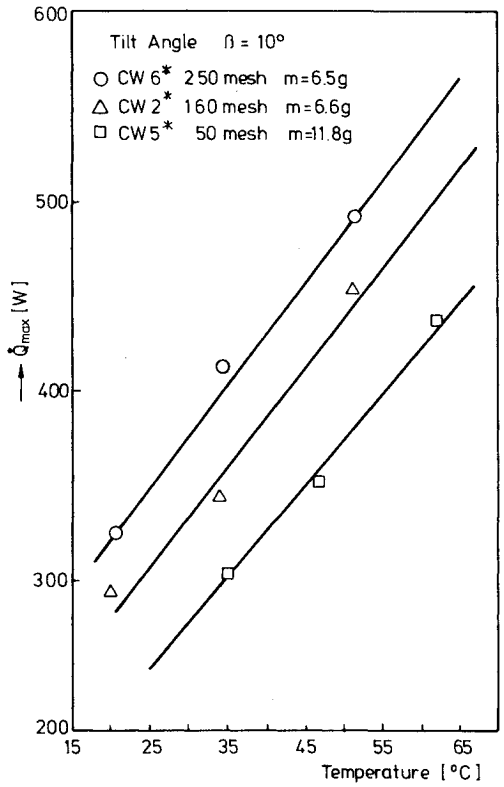

Fig. 15 Influence of screen mesh size on maximum heat-transport capability.

thickness δ. Moreover, drawing an analogy with pool boiling, the higher the friction force, the greater would be the bubble departure diameter and the smaller the magnitude of $\dot{q}''_{max}$.[10] We thus have $\dot{q}''_{max} \alpha(1/\delta)$. Nondimensionalizing using the wire thickness D_r, we obtain $\dot{q}''_{max} \alpha (D_r/\delta)$.

Combining the simultaneous influence of β, m, and n,

$$\dot{q}''_{max} = C_3 (\dot{V}_{total})^{0.424} (1/V_P) (V_S/V_E)^{0.727} (D_r/\delta)^{n_3} \quad (7)$$

or

$$F_H = \frac{\dot{q}''_{max} V_P}{(\dot{V}_{total})^{0.424} (V_S/V_E)^{0.727}} = C_3 (D_r/\delta)^{n_3} \quad (8)$$

The log-log plot in Fig. 14 shows the variation of F_H with (D_r/δ). The value of the exponent n_3 is computed as 0.96.

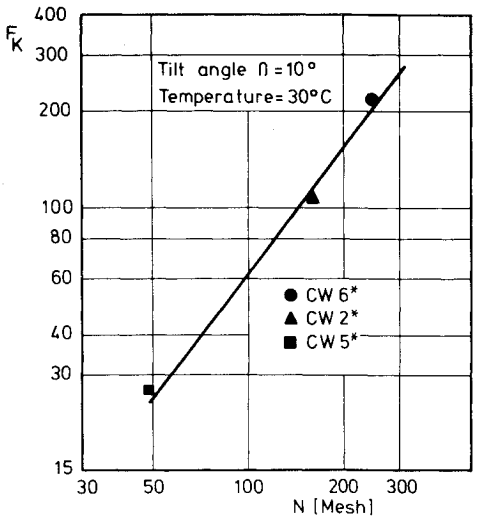

Fig. 16 Correlation between F_K and screen mesh size N.

Screen Mesh Size, N

Figure 15 presents the dependence of $\dot{Q}_{max}$ on operating temperature for three heat pipes (CW5*, CW2*, CW6*) lined with two layers of 50-, 160-, and 250-mesh wicks, respectively, on their inner walls. The tilt angle of all heat pipes considered here is 10 deg. Figure 15 indicates an increase in $\dot{Q}_{max}$ for heat pipes lined with a finer mesh, i.e., $\dot{Q}_{max} \alpha N$. As a finer mesh increases the capillary forces for condensate return, an increase in $\dot{Q}_{max}$ with N implies that capillary forces do play a role for condensate return in gravity-assisted heat pipes in spite of the presence of the strong gravity forces.

The combined influence of β, m, n, and N on $\dot{q}_{max}$ is then written as:

$$\dot{q}''_{max} = C_4 (\dot{V}_{total})^{0.424} (1/V_P) (V_S/V_E)^{0.727} (D_r/\delta) (N)^{n_4} \quad (9)$$

or

$$F_K = \frac{\dot{q}''_{max} V_P}{(\dot{V}_{total})^{0.424} (V_S/V_E)^{0.727} (D_r/\delta)} = C_4 (N)^{n_4} \quad (10)$$

The variation of F_K on screen mesh size N is seen to be linear on the log-log plot in Fig. 16. The exponent n_4 is calculated to be 1.35.

Operating Temperature, T_{11} or T_5

The heat pipe operating temperature is characterized either by the vapor temperature T_{11} or the temperature of the adiabatic section T_5. We have seen earlier in Figs. 8, 11, 13, and 15 that a strong dependence of $\dot{Q}_{max}$ on T_5 exists. This is essentially due to a considerable variation in the thermophysical properties of water in the temperature range considered in the present investigations.

The temperature influences the maximum heat flux $\dot{q}''_{max}$, both due to nucleate boiling and to impulse convection. To account for the influence due to nucleate boiling, we may use the pool boiling correlation presented by Kutateladze,[7] whereby

$$K_B = r\sqrt{\rho_l}\sqrt[4]{\sigma g(\rho_l - \rho_v)} \quad (11)$$

where r is the latent heat of vaporization, ρ is the density, σ is the surface tension, and the subscripts l and v represent the liquid and vapor phases, respectively. The influence due to impulse convection is more difficult to account for due to the nonavailability of any experimental data at the low velocities that are encountered here. Hence, we draw an analogy to flow boiling for liquid flow in a tube. In the case of flow boiling, Kutateladze[9] proposed that convective effects may be ac-

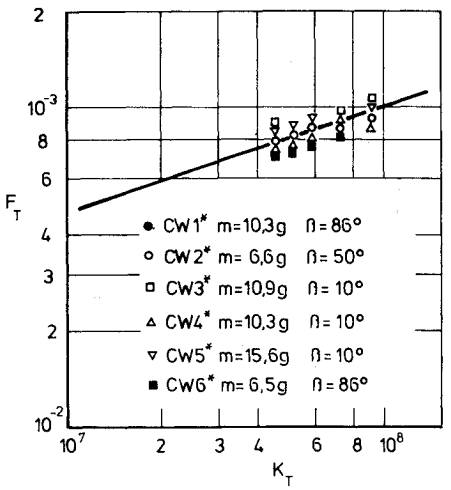

Fig. 17 Correlation between F_T and K_T for various heat pipes.

counted for by including a term in Eq. (11) which describes the ratio between the kinetic energy of the flowing liquid and the surface tension forces. For the conditions existing in the water heat pipes investigated here, this term is obtained as

$$K_K = [(\rho_l - \rho_v)/g\sigma]^{0.106} \tag{12}$$

The influence of temperature is then described by

$$K_T = K_B \cdot K_K \tag{13}$$

The combined influence of the five influence parameters β, m, n, N and T_{11} on $\dot{q}''_{\max}$ is then obtained as

$$\dot{q}''_{\max} = C_5 (\dot{V}_{\text{total}})^{0.424} (1/V_P)(V_S/V_E)^{0.727} (D_r/\delta)^{0.96} \times (N)^{1.35} (K_T)^{n_5} \tag{14}$$

or

$$F_T = \frac{\dot{q}''_{\max} V_P}{(\dot{V}_{\text{total}})^{0.424} (V_S/V_E)^{0.727} (D_r/\delta)^{0.96} (N)^{1.35}} = C_5 (K_T)^{n_5} \tag{15}$$

The values of the constant C_5 and the exponent n_5 are determined from the log-log plot of F_T vs K_T presented in Fig. 17. We obtain $C_5 = 0.025$ and $n_5 = 0.325$.

The data for limiting heat flux for the screen wick heat pipes of nominal diameter of 12.5 mm considered in the present study are hence correlated as

$$\dot{q}''_{\max} = 0.025 (\dot{V}_{\text{total}})^{0.424} (1/V_P)(V_S/V_E)^{0.727} (D_r/\delta)^{0.96} \times (N)^{1.35} (K_T)^{0.325} \ \text{W/m}^2 \tag{16}$$

where all the parameters are in MKS units.

Figure 18 shows a comparison between the correlation given by Eq. (16) and experimental data for heat pipe CW4* obtained with a fill charge of 13.3 g and tilt angle of 10 and 86 deg. Similar comparisons were carried out for 220 other data points. The agreement between the measured and computed value of the maximum heat flux density was found to be good; the discrepancy being less than ±10%.

VI. Comparison of the Gravity-Assisted Heat Pipes with Two-Phase Thermosyphon

To obtain an indication of the relative performance of wicked and nonwicked heat pipes, a two-phase thermosyphon

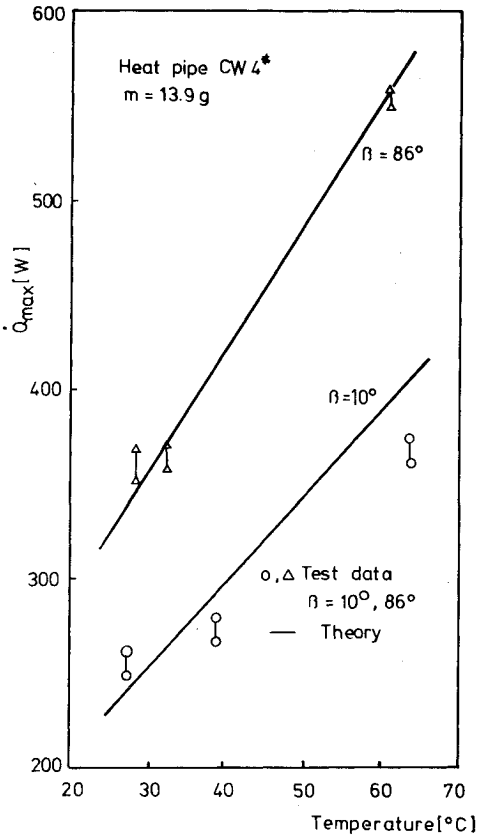

Fig. 18 Comparison between measured and predicted maximum heat-transport capability.

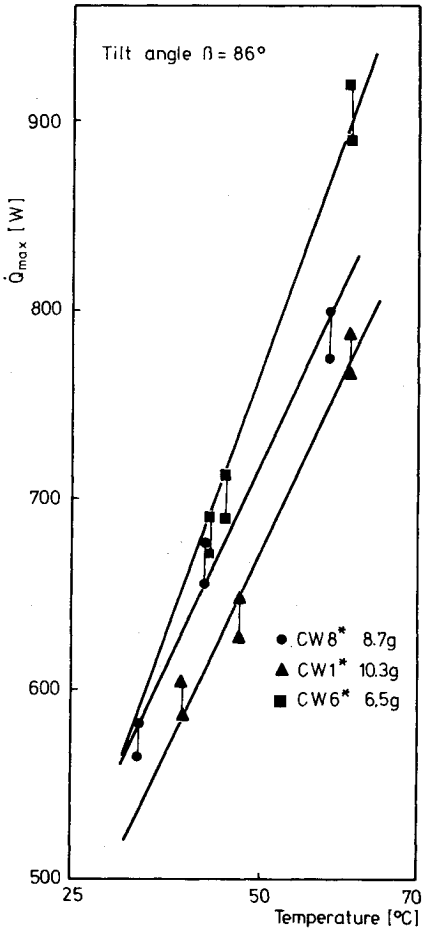

Fig. 19 Comparison of gravity heat pipes CW1* and CW8* with thermosyphon CW8*.

having the same dimensions as the heat pipes was constructed. The thermosyphon, coded as CW8* in Table 2, was filled with 8.7 g of water corresponding to 55% of the evaporator volume and tested at tilt angle of 10 and 86 deg. During operation of the thermosyphon, a liquid pool is present in a part of the evaporator zone and a thin liquid film flows down the remaining length of the thermosyphon due to the effect of gravity. As in gravity-assisted heat pipes with liquid overfill, the heat transfer in the evaporator zone during steady-state operation of the thermosyphon is influenced by nucleate boiling and impulse convection, while the heat-transfer limit is caused by the onset of film boiling.

Figure 19 provides a comparison of the maximum heat-transport capability, $\dot{Q}''_{max}$, measured with the thermosyphon CW8* and with the heat pipes CW1* (one-layer 160 mesh) and CW6* (two-layer 250 mesh). Figure 19 is for a tilt angle of 86 deg. It is of interest to note that $\dot{q}''_{max}$ achieved with the thermosyphon is of the same order of magnitude as the heat pipes; for an operating temperature of 40 °C, $\dot{q}''_{max}$ for the thermosyphon is 4% greater than that for CW1* and 7% less than that for CW6*.

VII. Summary

Visual observations and measurements with gravity-assisted heat pipes with liquid overfill have established that the steady-state heat transfer in the heat pipes is affected by nucleate boiling and impulse convection in the liquid pool present in the evaporator zone. The limitation to the heat pipe performance is caused by the onset of film boiling in this region.

The maximum heat-transport capability of the heat pipes, $\dot{q}''_{max}$, is measured as a function of several influence parameters and is found to increase with operating temperature, tilt angle, and screen mesh size, while decrease with the number of screen layers. On the other hand, the liquid overfill has only a weak influence on $\dot{q}''_{max}$.

The data for $\dot{q}''_{max}$ have been correlated using the theory of similarity and the combined influence of the parameters considered in the investigations has been obtained. Comparisons between the correlation curve for $\dot{q}''_{max}$ and 220 data points show the discrepancy to lie within ± 10%.

References

[1] Abhat, A. and Nguyen-Chi, H., "Investigation of Performance of Gravity-Assisted Copper-Water Heat Pipes," *Proceedings of the 2nd International Heat Pipe Conference,* Bologna, Italy, 1976, pp. 23-36.

[2] Kaser, R.V., "Heat Pipe Operation in a Gravity Field with Liquid Pool Pumping," Paper WD 1912, McDonnell Douglas Corp., Seattle, Wash., 1972.

[3] Bienert, W.B., Trimmer, D.S., and Wolf, D.A., "Application of Heat Pipes to Solar Collectors," *Proceedings of the 10th Intersociety Energy Conversion Engineering Conference,* Newark, Del., 1975, pp. 1533-1539.

[4] Kemme, J.E., "Vapor Flow Consideration in Conventional and Gravity-Assist Heat Pipe," *Proceedings of the 2nd International Heat Pipe Conference,* Bologna, Italy, 1976, pp. 11-22.

[5] König, A. and Gregorig, R., "On the Departure of Steam Bubbles under Conditions of Pool Boiling," *Wärme- und Stoffübertragung,* Vol. 3, 1973, pp. 165-174.

[6] Fritz, W. and Ende, W., "The Vaporization Process According to Cinema to Graphic Pictures of Vapor Bubbles," *Physik Zeitschrift,* Vol. 37, 1936, pp. 391-401.

[7] Kutateladze, S.S., "Heat Transfer in Condensation and Boiling," Publication of the State Scientific and Technical Publishers of Literature on Machinery, Moscow-Leningrad, 1952.

[8] Nguyen-Chi, H., "Untersuchung der Wärmeübertragung und Leistungsgrenzen in schwerkraftunterstützten Wärmerohren mit Netzstrukturen und Wasser als Wärmeträger," IKE Internal Report, Institut für Kernenergetik und Energiesysteme, Stuttgart, FRG (in prepartion).

[9] Kutateladze, S.S. and Bukarov, B.A., "The Critical Heat Flux for Natural Convection and Forced Flow of Boiling and Subcooled Dowtherm," Symposium *Problems of Heat Transfer and Hydraulics of Two Phase Media,* Pergamon Press, New York 1969, pp. 63-84.

[10] Borishanskii, V.M. and Fokin, B.S., "Calculation of Maximum Critical Heat Flux During Bubble Boiling in a Large Volume at Cylindrical and Spherical Surfaces," *Inzhenerno-Fizicheskii Zhurnal,* Vol. 28, No. 2, 1975, pp. 374-376.